Available online at www.sciencedirect.com
SCIENCE DIRECT®
Journal of Solid State Chemistry 177 (2004) 966–971
JOURNAL OF SOLID STATE CHEMISTRY
http://elsevier.com/locate/jssc

Magnesium substitution in $Nd_{0.7}Sr_{0.3}MnO_3$

M. Tseggai,[a,*] R. Mathieu,[a] P. Nordblad,[a] R. Tellgren,[a] L.V. Bau,[b] D.N.H. Nam,[b] N.X. Phuc,[b] N.V. Khiem,[c] G. André,[d] and F. Bourée[d]

[a] *The Ångstrom Laboratory, Solid State Physics Department of Engineering Sciences, Uppsala University, Uppsala SE 751 21, Sweden*
[b] *Institute of Materials Science, N.C.S.T., Nghiado-Caugiay-Hanoi, Viet Nam*
[c] *Department of Science and Technology, Hongduc University, Thanhhoa, Viet Nam*
[d] *Laboratoire Léon Brillouin, CEA-CNRS/ Saclay, Gif sur Yvette F-91 191, France*

Received 1 July 2003; received in revised form 23 September 2003; accepted 30 September 2003

Abstract

Magnesium substitution in $Nd_{0.7}Sr_{0.3}MnO_3$ has been studied by neutron powder diffraction. Polycrystalline samples of nominal compositions $Nd_{0.7}Sr_{0.3}Mn_{1-y}Mg_yO_3$ with $y = 0.0$, 0.1, 0.2 and 0.3 were synthesized by the standard solid-state reaction method. Rietveld refinements of the neutron powder diffraction data showed that all samples had distorted perovskite structure of orthorhombic symmetry. Mg initially preferred to substitute for Nd and only at Mg concentration greater than 0.1, a substantial substitution for Mn occurred. Our study also showed that Mg-substitution did not change the crystal structure of $Nd_{0.7}Sr_{0.3}MnO_3$.

Keywords: Mg-substitution; Neutron powder diffraction; Perovskite manganites; Double exchange mechanism; Neodymium strontium manganese oxide ($Nd_{0.7}Sr_{0.3}MnO_3$)

1. Introduction

The perovskite manganites, which have the general formula $T_{1-x}D_xMnO_3$ ($T = La^{3+}$, Pr^{3+}, or Nd^{3+} and $D = Ca^{2+}$, Sr^{2+}, Ba^{2+}, or Pb^{2+}), have been found to have intriguing magnetic and transport properties [1–4]. Since this discovery, more than a decade ago, perovskite manganites have attracted considerable attention not only in fundamental science, but also in industry due to a potential applicability in devices such as magnetic recording heads. The properties of perovskite manganites are sensitively dependent on their stoichiometry and structure. In the insulating $TMnO_3$, Mn exists as Mn^{3+}, but by partial substitution of any of the divalent alkaline-earth ions for T^{3+}, some Mn^{3+} ions are converted to Mn^{4+} and this introduces a mixed valence state, which dramatically changes the magnetic and the transport properties of the materials. For example, replacing 30% of T^{3+} with D^{2+}, introduces a ferromagnetic state at low temperatures, which is accompanied by a dramatic drop in the electrical resistance of the materials. In addition, such ferromagnets exhibit the colossal magnetoresistance (CMR) effect [5]. The substitution concentration x and the average A-site ion radius $\langle r_A \rangle$ control the transition temperatures [6–9] of these materials. (The general formula of the perovskite structure is ABO_3, and accordingly the $T_{1-x}D_x$ ions are in the A-site and the Mn ions in the B-site.) The CMR effect of perovskite manganites can be explained in terms of the ferromagnetic double exchange (DE) mechanism [10,11], which involves the overlapping of manganese incomplete d-shells and oxygen p-shells, and is mediated by hopping of charge carriers along the Mn–O–Mn bonds of the lattice. The mechanism is dramatically influenced by small changes in the Mn–Mn distances and the Mn–O–Mn bond angles [12]. The objectives of studying Mg substitution in $Nd_{0.7}Sr_{0.3}MnO_3$ are to find out for which of the constituent element(s) Mg substitutes and how the structure is affected by the substitution. Neutron diffraction is very suitable for these purposes; and favorable for investigated system determination of the site occupancies since the scattering amplitude for Mn is negative (−3.73 fm) while the scattering amplitudes for Nd, Sr and Mg are positive: +5.38, +7.69 and +7.02 fm, respectively. We believe that this structural knowledge can help to understand the

*Corresponding author. Fax: +46-0-18-50-01-31.
E-mail address: mehreteab.tseggai@angstrom.uu.se (M. Tseggai).

0022-4596/$ - see front matter © 2003 Elsevier Inc. All rights reserved.
doi:10.1016/j.jssc.2003.09.044

effects of Mg substitution on the physical properties of $Nd_{0.7}Sr_{0.3}MnO_3$.

The magnetic and transport properties of Mg substituted $Nd_{0.7}Sr_{0.3}MnO_3$ have been studied by, e.g., Nam et al. [13]. They have found that for Mg substitutions up to $y = 0.1$, the system remains ferromagnetic and metallic at low temperatures and shows the CMR effect close to T_c, however, with a monotonous decrease of T_c from 235 K for the pure compound to 180 K for the $y = 0.1$ sample. Sample of composition $y \geqslant 0.2$ on the other hand showed a spin glass like behavior at low temperatures and remained insulating also in the low temperature phase. The observed spin glass like maximum in the zero-field-cooled susceptibility occurred at a temperature below 50 K already for the $y = 0.2$ sample. All these observations indicate a weakening of the ferromagnetic DE interaction and an increased influence of the antiferromagnetic (AF) super exchange with increasing Mg substitution. Evidence that competition between ferromagnetic DE and AF super exchange is important even in the parent compound $Nd_{0.7}Sr_{0.3}MnO_3$ is found from the occurrences of magnetic aging and non-equilibrium dynamics in its ordered ferromagnetic state [14].

2. Experiments

Polycrystalline samples of compositions $Nd_{0.7}Sr_{0.3}Mn_{1-y}Mg_yO_3$ with $y = 0.0$, 0.1, 0.2 and 0.3 were synthesized by the standard solid-state reaction method. The starting compound ($Nd_{0.7}Sr_{0.3}MnO_3$) was prepared as follows: powders of Nd_2O_3, $SrCO_3$ and MnO_2 in stoichiometric proportions were mixed in ethanol and the mixed powder was pressed into pellets and calcinated at 1423 K in air atmosphere for two weeks with several intermediate grindings. The calcinated pellets were sintered at 1623 K for 5 h and then cooled down to room temperature (298 K).

Each of the three samples (with $y = 0.1$, 0.2, and 0.3) was also fabricated by the standard solid-state reaction method. Powders of Nd_2O_3, $SrCO_3$, MgO and MnO_2 in stoichiometric proportions were mixed in ethanol and the mixed powder was pressed into pellets and calcinated at 1323 K in air atmosphere for 23 h and then cooled down to room temperature (298 K) by switching off the furnace. The calcinated pellets were sintered first at 1573 K for 45 h and then at 1623 K for 7 h. After that the pellets were first cooled down slowly to 573 K and finally cooled to room temperature by switching off the furnace. X-ray powder diffraction showed single-phase orthorhombic perovskite structure of space group *Pnma*, No 62 for all the samples.

The neutron powder diffraction data were collected at the Orphée reactor, Laboratoire Léon Brillouin, CEA-CNRS, Saclay, France. Neutron data of the four samples were recorded on the high-resolution 2-axes diffractometer 3T2 with 20 detectors using the wavelength, $\lambda = 1.2251$ Å. The pattern was recorded at room temperature (298 K) over the angular range $6.00^\circ \leqslant 2\vartheta \leqslant 125.70^\circ$ with a step length of 0.05° in 2ϑ.

3. Results and discussions

The neutron powder diffraction data of the four samples were analyzed with Rietveld technique using the computer program FullProf [15]. Simultaneous refinement of both thermal and occupancy parameters was not possible since they are almost 100% correlated to each other. However, chemical analysis of the samples showed that there was a lack of neodymium (of almost constant amount) in all substituted samples and that the manganese content was substantially reduced only in the samples with higher Mg-substitution, i.e., $y > 0.1$. The strontium and oxygen contents, however, remained unaffected by Mg-substitution for all values of y. With this information in mind, the refinements were carried out letting Mg substitute for both Nd and Mn. The occupancies were then varied stepwise, but kept fixed in each refinement. The final results were taken from the cycles with the lowest R-value and the most realistic values for the thermal parameters. The results of the Rietveld analysis are summarized in Table 1.

The Rietveld analysis of the neutron data showed that the samples were all pure single phased with an orthorhombic perovskite structure, space group *Pnma*, No. 62. We have not observed any appreciable differences neither in the diffraction patterns nor in the crystal structures and hence the neutron diffractogram shown in Fig. 1 and the crystal structure in Fig. 2 are representatives for all the samples. The Mn ions are surrounded by oxygen in an octahedral coordination as illustrated in Fig. 3. The orthorhombic lattice parameters are related to the simple cubic perovskite lattice parameter ($a_p = 3.86$ Å) by $a \approx c \approx (\sqrt{2})a_p$, $b \approx 2a_p$ (cf. Table 1). The variations of the lattice parameters as a function of Mg-substitution are plotted in Fig. 4a. The lattice parameters monotonously decreased with increasing Mg substitution and consequently a monotonous decrease of the unit cell volume from 230.09(1) $Å^3$ for $y = 0.0$ to 228.25(4) $Å^3$ for $y = 0.3$ was observed. The thermal parameters and the occupancies (indicated in the chemical formulas) of the different constituent atoms obtained from Rietveld analysis are shown in Table 1. In the Mg-substituted samples, the occupancy for Nd remained constant at 0.6 but for Mn the occupancy started to decrease noticeably only at $y > 0.1$.

To discuss details of the distortion induced by Mg substitution in the structure in general and the oxygen octahedral structure in particular, we need to look into

Table 1
Room temperature structures of $Nd_{0.7}Sr_{0.3}MnO_3$ samples without and with Mg substitution

Space Group: *Pnma*, No. 62

$Nd_{0.7}Sr_{0.3}MnO_3$
Cell parameters (in Å)
$a = 5.4583(2)$
$b = 7.7118(2)$
$c = 5.4663(3)$
Cell Volume = 230.09(1) Å^3
Atomic coordinates and thermal parameters

	x	y	z	BISO
A	0.0254(2)	0.25	−0.0060(4)	0.86(2)
B	0	0	0.5	0.65(2)
O1	0.4907(4)	0.25	0.0653(4)	1.38(1)
O2	0.2794(3)	0.0335(2)	0.7212(3)	1.38(1)

Reliability factors
$R_p = 3.3\%$
$R_{wp} = 4.2\%$
$\chi^2 = 2.8$

$Nd_{0.6}Mg_{0.1}Sr_{0.3}MnO_3$
Cell parameters (in Å)
$A = 5.4521(2)$
$b = 7.7046(3)$
$c = 5.4647(2)$
Cell Volume = 229.55(2) Å^3
Atomic coordinates and thermal parameters

	x	y	z	BISO
A	0.0238(3)	0.25	−0.0047(5)	0.70(2)
B	0	0	0.5	0.97(3)
O1	0.4915(5)	0.25	0.0640(5)	1.33(2)
O2	0.2778(3)	0.0325(2)	0.7217(3)	1.33(2)

Reliability factors
$R_P = 3.8\ \%$
$R_{WP} = 5.0\%$
$\chi^2 = 3.4$

$Nd_{0.6}Mg_{0.1}Sr_{0.3}Mn_{0.9}Mg_{0.1}O_3$
$a = 5.4466(4)$
$b = 7.7003(5)$
$c = 5.4600(4)$
Cell volume = 228.99(3) Å^3
Atomic coordinates and thermal parameters

	x	y	z	BISO
A	0.0247(3)	0.25	−0.0056(6)	0.62(2)
B	0	0	0.5	0.70(4)
O1	0.4930(6)	0.25	0.0664(6)	1.43(2)
O2	0.2746(5)	0.0317(3)	0.7206(3)	1.43(2)

Reliability factors
$R_P = 3.7\ \%$
$R_{WP} = 4.8\ \%$
$\chi^2 = 3.3$

$Nd_{0.6}Mg_{0.1}Sr_{0.3}Mn_{0.8}Mg_{0.2}O_3$
$a = 5.4424(5)$
$b = 7.6919(7)$
$c = 5.4523(5)$
Cell volume = 228.25(4) Å^3
Atomic coordinates and thermal parameters

	x	y	z	BISO
A	0.0253(3)	0.25	−0.0063(7)	0.49(2)
B	0	0	0.5	0.62(5)
O1	0.4933(7)	0.25	0.0646(9)	1.38(2)
O2	0.2743(6)	0.0340(4)	0.7200(5)	1.38(2)

Reliability factors
$R_P = 4.2\ \%$
$R_{WP} = 5.5\ \%$
$\chi^2 = 4.0$

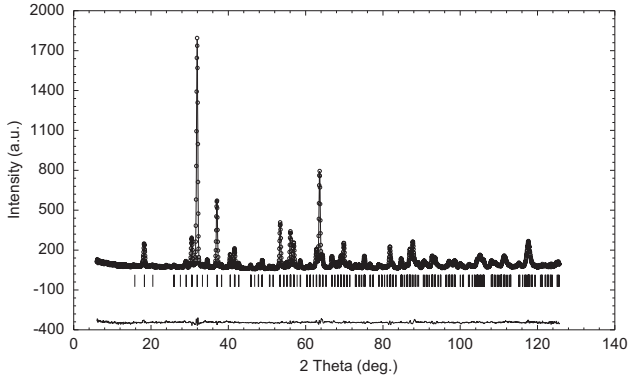

Fig. 1. A representative plot of the Rietveld refinement of the neutron data for $Nd_{0.6}Mg_{0.1}Sr_{0.3}Mn_{0.9}Mg_{0.1}O_3$ at 298 K. In the plot, the points are the observed data; the solid line is the calculated intensity; the small vertical lines are the positions of Bragg reflections and the lower line is the difference curve, $Y_{obs} - Y_{calc}$.

the charge balance and ionic radii of the different ions. Using the derived compositions for the different samples, the compositions of ionic crystals can be labeled as

$Nd^{3+}_{0.7}\,Sr^{2+}_{0.3}\,Mn^{3+}_{0.7}\,Mn^{4+}_{0.3}\,O^{2-}_3$ for $(y = 0.0)$,

$Nd^{3+}_{0.6}\,Mg^{2+}_{0.1}\,Sr^{2+}_{0.3}\,Mn^{3+}_{0.6}\,Mn^{4+}_{0.4}\,O^{2-}_3$ for $(y = 0.1)$,

$Nd^{3+}_{0.6}\,Mg^{2+}_{0.1}\,Sr^{2+}_{0.3}\,Mg^{2+}_{0.1}\,Mn^{3+}_{0.4}\,Mn^{4+}_{0.5}\,O^{2-}_3$ for $(y = 0.2)$,

$Nd^{3+}_{0.6}\,Mg^{2+}_{0.1}\,Sr^{2+}_{0.3}\,Mg^{2+}_{0.2}\,Mn^{3+}_{0.2}\,Mn^{4+}_{0.6}\,O^{2-}_3$ for $(y = 0.3)$.

The ionic radii which may contribute to the shrinkage and distortion of the structure are $R^{3+}_{Nd} = 1.27$ Å, $R^{2+}_{Mg} = 0.72$ Å, $R^{3+}_{Mn} = 0.65$ Å and $R^{4+}_{Mn} = 0.53$ Å [16]. In addition, the DE mechanism remains effective for the $y = 0.1$ sample, since almost no Mg^{2+} ions occupy the *B*-site and the content of Mn^{4+} is within the range $0.2 \leqslant Mn^{4+} \leqslant 0.5$, where DE is effective in $Nd_{0.7}Sr_{0.3}MnO_3$. Using this information and starting from the structural property of the parent compound $Nd_{0.7}Sr_{0.3}MnO_3$, we can understand why the lattice parameters decreased continuously and monotonously with increasing Mg-substitution as follows:

(1) For $y = 0.1$, the decrease of the lattice parameters is mainly due to the replacement of the large Nd^{3+}

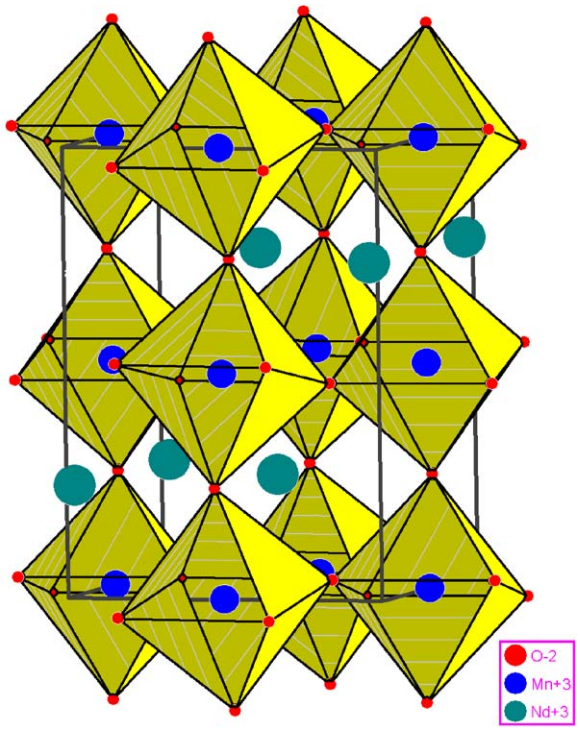

Fig. 2. The crystal structure of $Nd_{0.6}Mg_{0.1}Sr_{0.3}Mn_{0.9}Mg_{0.1}O_3$ at room temperature.

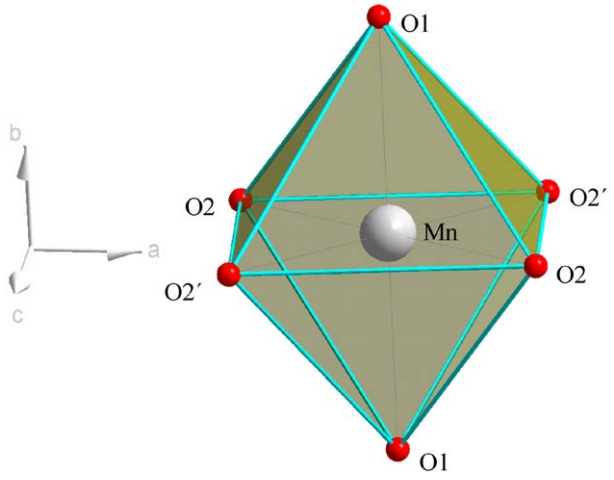

Fig. 3. An octahedron with manganese in the centre and oxygen atoms at the corners.

ions by smaller Mg^{2+} ions. The decrease of Mn^{3+} content as a result of its conversion into Mn^{4+} has a marginal effect on the cell parameters.

(2) For $y = 0.2$ and 0.3, the replacement of Mn^{3+} ions with Mg^{2+} greatly weakens the DE interaction. The content of the Mn^{4+} ions increases due to the conversion of Mn^{3+} into Mn^{4+} and the content of the Mn^{3+} ions additionally reduces due to its replacement by Mg^{2+} ions. This resulted in a

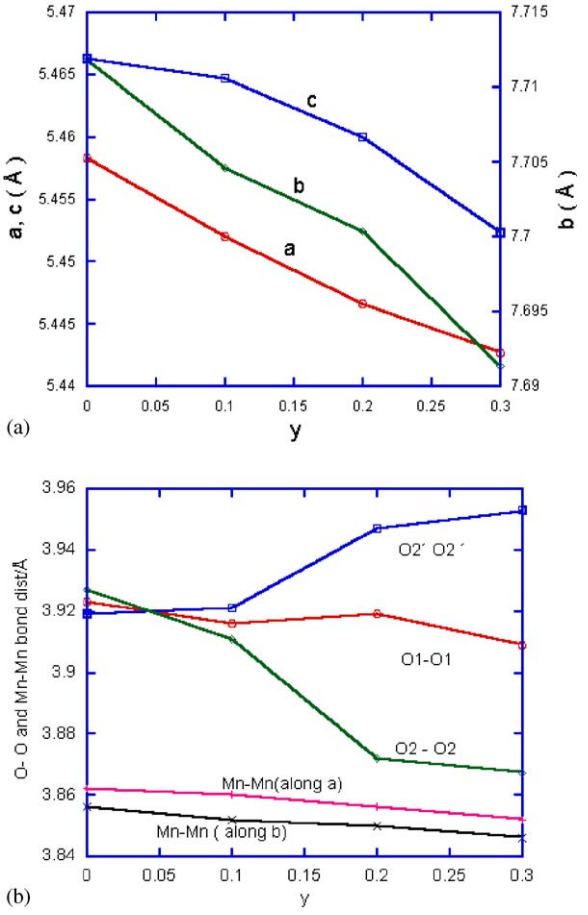

Fig. 4. (a) Changes of cell parameters as the function of Mg-substitution and (b) variations of O–O and Mn–Mn distances as a function of Mg-substitution.

shrinkage and distortion of the octahedral structure. The *B*-site is now occupied by three different ions, Mn^{4+}, Mn^{3+} and Mg^{2+} where Mn^{4+} ions are in majority. The increase of the content of the small Mn^{4+} ions coupled with their large charge is the main cause for the decrease of the lattice parameters and the distortion of the octahedron in the $y = 0.2$ and 0.3 samples.

(3) Looking further into the oxygen octahedron, the changes in O–O distances can be discussed with the help of Fig. 3. Note that O1–O1 is the distance between the two oxygen atoms located at the apices of the octahedron along the *b*-direction, and the O2–O2 and O2′–O2′ are the distances between oxygen atoms along the diagonals of the quadrilateral lying almost parallel to the *ac*-plane. Also note that the O2 and O2′ atoms are in equivalent crystallographic positions and they are labeled differently only for clarity. The O1–O1, O2–O2, and O2′–O2′ are plotted as a function of Mg substitution in Fig. 4b. The O1–O1 length which was shortened from 3.923(1) Å for $y = 0.0$ to 3.911(2) Å for $y = 0.3$ made the octahedral shrink

slightly. However, the O2–O2 and O2′–O2′ distances were markedly affected by the Mg substitution to cause noticeable distortion in the octahedron. The O2–O2 diagonal was shortened from 3.927(3) Å for $y = 0.0$ to 3.867(6) Å for $y = 0.3$ and the O2′–O2′ diagonal was elongated from 3.919(3) Å for $y = 0.0$ to 3.954(6) Å for $y = 0.3$. The small Mn^{4+} ions and their large charge are the main cause of the octahedral distortion at $y = 0.2$ and 0.3 since they occupy several *B*-site positions and the small Mn^{4+} radius does not allow all oxygen atoms to come equally close.

The Mn–Mn nearest distances along the *b*-axis and in the *ac*-plane are also plotted as a function of Mg substitution in Fig. 4b. These distances are shortened in same proportions as the lattice parameters do with increase of Mg-substitution. Nevertheless, the changes observed in the O–O and Mn–Mn distances did not cause any significant change in the crystal structure of the materials since all were found to have the same orthorhombic perovskite structure as confirmed by Rietveld analysis of the neutron data.

All the O–Mn–O bond angles along the diagonals are equal to 180° as a consequence of the space group symmetry. The O1–Mn–O2′, O1–Mn–O2 and O2′–Mn–O2 bond angles deviated slightly from 90° as a consequence of the asymmetry of the octahedron. The O–Mn–O bond angles remained almost unchanged with increasing Mg-substitution.

The Mn–O1–Mn bond angle is close to 159° for all values of *y* (Table 2), which is a measure of the tilting of the octahedra as compared to the undistorted ideal cubic perovskite structure (Mn–O1–Mn = 180° in the cubic perovskite structure).

The neodymium ions, which are coordinated with twelve oxygen ions, fill up the space between the octahedra (see Fig. 2). The Nd–O bond lengths are different in the orthorhombic perovskite structure. We can classify them into short, medium, and long bonds. According to this classification there are four short Nd–O bond lengths between 2.404 and 2.581 Å, four medium Nd–O bond lengths between 2.614 and 2.733 Å, and four long Nd–O bond lengths between 2.921 and 3.158 Å. These bond lengths are differently affected by Mg substitution: some are elongated and others are shortened, but the net effect resulted in shrinkage of the Nd (*A*-site) coordination geometry.

Table 2
Bond distances (in Å) and bond angles (in degrees) for different values of *y*

y	0	0.1	0.2	0.3
O1–O1	3.923(1)	3.916(1)	3.919(1)	3.911(2)
O2′–O2′	3.919(3)	3.921(3)	3.947(4)	3.954(6)
O2–O2	3.927(3)	3.911(3)	3.872(5)	3.867(6)
Mn–Mn (*b*-direction)	3.8559(1)	3.8523(2)	3.8502(3)	3.8456(4)
Mn–Mn (ac-plane)	3.8626(2)	3.8594(1)	3.8561(3)	3.8519(4)
O1–Mn–O2′	89.77(8)	89.90(9)	90.5(1)	89.9(2)
O1–Mn–O2	89.84(8)	89.83(9)	89.6(1)	90.4(2)
O2′–Mn–O2	91.09(2)	91.05(2)	90.91(2)	90.97(3)
Mn–O1–Mn (*b*-direction)	158.9(1)	159.3(2)	158.7(2)	159.5(3)

4. Conclusions

Rietveld analysis of the neutron diffraction data showed that the Mg substituted samples were of compositions $Nd_{0.6}Mg_{0.1}Sr_{0.3}MnO_3$, $Nd_{0.6}Mg_{0.1}Sr_{0.3}Mn_{0.9}Mg_{0.1}O_3$, and $Nd_{0.6}Mg_{0.1}Sr_{0.3}Mn_{0.8}Mg_{0.2}O_3$, and not the expected compositions $Nd_{0.7}Sr_{0.3}Mn_{1-y}Mg_yO_3$ with *y* in the range $0.1 \leqslant y \leqslant 0.3$. This implies that Mg substituted for both Nd and Mn.

Another important result of our study of Mg-substitution in $Nd_{0.7}Sr_{0.3}MnO_3$ is that we are able to derive structural information that implies that the DE mechanism should be weakly affected by substitutions up to $y = 0.1$, since substitution on the *A*-site mainly weakens the DE interaction only by introducing additional disorder (we find no systematic change of the Mn–O–Mn bond angle with increasing Mg substitution). Whereas, the DE should be strongly suppressed once Mg starts to substitute on the *B*-sites, since it then directly interrupts hopping possibilities for the e_g electrons and also alters the hole concentration more strongly. These indications of a non-monotonous weakening of the DE on increasing Mg substitution are in agreement with the corresponding changes of the physical properties of Mg doped $Nd_{0.7}Sr_{0.3}MnO_3$, as recalled above in the introduction.

Mg substitution in $Nd_{0.7}Sr_{0.3}MnO_3$ resulted in a continuous decrease of the cell parameters and hence the volume of the unit cells. It also caused some slight structural distortion in spite of which, however, all samples were found to be single-phased with orthorhombic perovskite structure of space group *Pnma*, No 62 as confirmed by Rietveld analysis.

Acknowledgments

The financial support from Sida/SAREC is gratefully acknowledged. Many thanks are also due to the Centre Culturel Suèdois in Paris for contribution to the French-Swedish collaboration. The authors are indebted to Dr. Jean Pettersson, Uppsala University, Department of Analytical Chemistry, for performing chemical analysis on the samples.

References

[1] A.P. Ramirez, J. Phys. Condens. Matter 9 (1997) 8171–8199.
[2] R. von Helmolt, J. Wecker, B. Holzapfel, L. Schultz, K. Samwer, Phys. Rev. Lett. 71 (1993) 2331–2333.
[3] S. Jin, T.H. Tiefel, M. McCormack, R.A. Fastnacht, R. Ramesh, L.H. Chen, Science 264 (1994) 413–415.
[4] G.H. Jonker, J.H. Van Santen, Physica (Utrecht) 16 (1950) 337–349; J. H. Van Santen, G. H. Jonker, Physica (Utrecht) 16 (1950) 599–600.
[5] P. Schiffer, A.P. Ramirez, W. Bao, S.-W. Cheong, Phys. Rev. Lett. 75 (1995) 3336–3339.
[6] R. Mahesh, R. Mahendiran, A.K. Raychaudhuri, C.N.R. Rao, J. Solid State Chem. 120 (1995) 204–207.
[7] A. Urushibara, Y. Moritomo, T. Arima, A. Asmatitsu, G. Kido, Y. Tokura, Phys. Rev. B 51 (1995) 14103–14109.
[8] H.Y. Hwang, T.T.M. Palstra, S.-W. Cheong, B. Batlogg, Phys. Rev. B 52 (1995) 15046–15049.
[9] P.G. Radaelli, M. Marezio, H.Y. Hwang, S.-W. Cheong, J. Solid State Chem. 122 (1996) 444–447.
[10] C. Zener, Phys. Rev. 82 (1951) 403–405.
[11] P.G. deGennes, Phys. Rev. 118 (1960) 141–154.
[12] A. Maignan, B. Raveau, Z. Phys. B 102 (1997) 299–305.
[13] D.N.H. Nam, R. Mathieu, P. Nordblad, N.V. Khiem, N.X. Phuc, J. Magn. Magn. Mater. 226 (2000) 1340–1341.
[14] D.N.H. Nam, R. Mathieu, P. Nordblad, N.V. Khiem, N.X. Phuc, Phys. Rev. B 62 (2000) 1027–1032.
[15] J. Rodriguez-Carvajal, ILL Internal Report, Computer Program FullProf.
[16] R.D. Shannon, Acta Crystallogr. A 32 (1976) 751–767.